

# PCCP

Accepted Manuscript



This is an *Accepted Manuscript*, which has been through the Royal Society of Chemistry peer review process and has been accepted for publication.

*Accepted Manuscripts* are published online shortly after acceptance, before technical editing, formatting and proof reading. Using this free service, authors can make their results available to the community, in citable form, before we publish the edited article. We will replace this *Accepted Manuscript* with the edited and formatted *Advance Article* as soon as it is available.

You can find more information about *Accepted Manuscripts* in the [Information for Authors](#).

Please note that technical editing may introduce minor changes to the text and/or graphics, which may alter content. The journal's standard [Terms & Conditions](#) and the [Ethical guidelines](#) still apply. In no event shall the Royal Society of Chemistry be held responsible for any errors or omissions in this *Accepted Manuscript* or any consequences arising from the use of any information it contains.

## ARTICLE

# Formation of fluorescent polydopamine dots from hydroxyl radical-induced degradation of polydopamine nanoparticles.

Cite this: DOI: 10.1039/x0xx00000x

Jia-Hui Lin,<sup>a</sup> Cheng-Ju Yu,<sup>a</sup> Ya-Chun Yang<sup>a</sup> and Wei-Lung Tseng<sup>\*a,b</sup>Received 00th January 2012,  
Accepted 00th January 2012

DOI: 10.1039/x0xx00000x

www.rsc.org/

This study describes the synthesis of fluorescent polydopamine dots (PDs) through hydroxyl radical-induced degradation of polydopamine nanoparticles. The decomposition of polydopamine nanoparticles to fluorescent PDs was confirmed using transmission electron microscopy and dark-field microscopy. The analysis of PDs by using matrix-assisted laser desorption/ionization time-of-flight mass spectrometry revealed that the PDs consisted of dopamine, 5,6-dihydroxyindole, and trihydroxyindole units. Oligomerization and self-assembly of these units produced a broad adsorption band, resulting in an excitation-wavelength-dependent emission behavior. The maximal fluorescence of PDs appeared at 440 nm with a quantum yield of 1.2%. The coordination between the catechol groups of PDs and ferric ions ( $\text{Fe}^{3+}$ ) quenched the fluorescence of PDs; the limit of detection at a signal-to-noise ratio of 3 for  $\text{Fe}^{3+}$  was determined to be 0.3  $\mu\text{M}$ . The presence of pyrophosphate switched on the fluorescence of the PDs- $\text{Fe}^{3+}$  complexes. Compared to the other reported methods for sensing  $\text{Fe}^{3+}$ , PDs provided the simple, low-cost, and reusable detection of  $\text{Fe}^{3+}$ .

## 1. Introduction

Various organic dyes are widely used in biological imaging and biosensors.<sup>1, 2</sup> However, limitations of these dyes, such as broad emission spectra, poor photostability, small Stokes shifts, and a short fluorescence lifetime, have been recognized.<sup>3</sup> Recently, fluorescent nanoparticles including semiconductor-, silica-, and carbon-based quantum dots,<sup>4-6</sup> metal nanoclusters,<sup>7</sup> and polymer dots,<sup>2</sup> have been developed to address the aforementioned limitations. They are extensively applied in the fields of drug delivery, biosensors, bioimaging, and biomedical sciences. For example, semiconductor quantum dots exhibit broad excitation spectra and size-tunable light emission; thus, semiconductor quantum dots of different colors can be excited for multiplexed bio-detection on solid-state microarrays.<sup>8</sup> Carbon-based nanomaterials exhibit size-, excitation-, pH-, solvent-, and concentration-dependent fluorescence, leading to the development of various biosensors.<sup>9-11</sup> The two-photon absorption cross section of gold nanoclusters is superior to that of many organic chromophores; thus, these nanoclusters are efficient absorbers for multiphoton biological imaging.<sup>12</sup> Polymer dots consisting of  $\pi$ -conjugated polymers exhibit extraordinary fluorescence brightness and excellent photostability; therefore, they can be used as optic probes for fluorescence imaging and flow cytometry.<sup>13, 14</sup>

Dopamine is capable of self-polymerizing to generate surface-adherent and biocompatible polydopamine films on all types of inorganic and organic substrates, such as metal/metal oxide nanoparticles,<sup>15, 16</sup> superhydrophobic surfaces,<sup>17</sup> and fluorescent nanoparticles.<sup>18</sup> The mechanism underlying the self-polymerization of dopamine is the oxidation of catechol to dopaminequinone under an aerobic and alkaline condition.<sup>19, 20</sup> In addition, polydopamine has optical properties similar to those of naturally occurring eumelanin. Under ultraviolet (UV) excitation, polydopamine exhibits a fluorescence peak at 400–500 nm and an excitation-wavelength-

dependent emission behavior. Although polydopamine has distinct advantages of biocompatibility and fluorescence properties, relative to the number of studies on other fluorescent nanoparticles, few studies have reported the preparation of fluorescent polydopamine nanoparticles. Zhang and colleagues proposed a top-down approach for preparing fluorescent polydopamine nanoparticles.<sup>21</sup> First, large polydopamine particles are obtained by adding dopamine to an alkaline solution. The formed polydopamine particles react with  $\text{H}_2\text{O}_2$  to produce fluorescent polydopamine nanoparticles. Chen and colleagues developed a multistep approach for generating fluorescent polydopamine capsules through the self-polymerization of dopamine on sacrificial templates and  $\text{H}_2\text{O}_2$ -induced oxidation of polydopamine.<sup>22</sup> Quignard et al. used UV light to illuminate polydopamine-coated emulsion droplets, resulting in the production of fluorescent polydopamine on the surface of emulsion droplets.<sup>23</sup>

The reaction of dopamine with hydroxyl radicals produced 2-hydroxyldopamine, 5-hydroxyldopamine, and 6-hydroxyldopamine.<sup>24</sup> We proposed that hydroxyl radicals could cause the addition of hydroxyl groups to polydopamine nanoparticles, which breaks down them into fluorescent polydopamine dots (PDs) through the reduction of  $\pi$ - $\pi$  stacking interaction between the oligomeric units in a polydopamine nanoparticles. Here, this study demonstrated that polydopamine nanoparticles can rapidly react with the hydroxyl radicals to produce blue-emitting PDs. In addition, we revealed that these blue-emitting PDs can sense ferric ions ( $\text{Fe}^{3+}$ ) in an aqueous solution through the coordination between  $\text{Fe}^{3+}$  and the catechol groups.

## 2. Materials and Methods

### 2.1 Chemicals and Materials.

Dopamine hydrochloride (purity of 99%), NaOH (purity of 97%),  $\text{FeCl}_2$ ,  $\text{FeCl}_3$ , LiCl, NaCl, KCl,  $\text{MgCl}_2$ ,  $\text{CaCl}_2$ ,  $\text{SrCl}_2$ ,  $\text{BaCl}_2$ ,  $\text{MnCl}_2$ ,  $\text{CoCl}_2$ ,  $\text{NiCl}_2$ ,  $\text{CuCl}_2$ ,  $\text{ZnCl}_2$ , and  $\text{CrCl}_3$  were

purchased from Acros Organics (Geel, Belgium).  $\text{Cd}(\text{ClO}_4)_2$ ,  $\text{HgCl}_2$ ,  $\text{Pb}(\text{NO}_3)_2$ , tris(hydroxymethyl)aminomethane (tris), sodium pyrophosphate,  $\text{H}_2\text{O}_2$  (purity of 30%) and  $\text{HCl}$  were ordered from Sigma-Aldrich (St. Louis, MO). Dialysis tubing (1 kDa MWCO) was obtained from Spectrum Laboratories, Inc. (Houston, Texas, USA). Water used in all of the experiments was doubly distilled and purified by a Milli-Q system (Millipore, Milford, MA, USA).

## 2.2 Synthesis of PDs.

The preparation of polydopamine was performed by dissolving dopamine hydrochloride (0.2 g) in  $\text{NaOH}$  (100 mL, 20 mM). The neutralized solution was heated at  $50^\circ\text{C}$  for 20 h under gentle stirring. The resulting solution was aged for two weeks. The obtained product (25 mL;  $\text{pH} \sim 7.5$ ) was added to a solution ( $\text{pH} \sim 10$ ) containing  $\text{H}_2\text{O}_2$  (20%, 15 mL) and  $\text{NaOH}$  (2.5 M, 10 mL). When the resulting solution ( $\text{pH} \sim 10.4$ ) was heated to reflux for 30 min, its color changed from black to yellow. The reaction mixture was cooled to room temperature and then dialyzed (molecular weight cutoff of 3000 Da) against 10% ethanol for one day; the role of ethanol is to act as hydroxyl radical scavenger.<sup>21</sup> The ready-to-use solution of the purified products ( $\text{pH} \sim 8.4$ ) was stored at  $4^\circ\text{C}$ . To calculate the concentration of PDs, the purified products were dried using a Vacuum centrifugal vaporizer (CVE-100, EYELA, Tokyo, Japan) with a cold trap (UT-3000, EYELA, Tokyo, Japan). The collected products were weighed using an analytical balance. The concentration of PDs was estimated to be  $0.27 \text{ mg mL}^{-1}$ .

## 2.3 Characterization of Polydopamine and PDs.

The absorption and fluorescence spectra were recorded using a double-beam UV-Vis spectrophotometer (V-670, JASCO, Tokyo, Japan) and a Hitachi F-7000 fluorometer (Hitachi, Tokyo, Japan), respectively. The images of transmission electron microscopy (TEM) were taken using a JEM-2100 transmission electron microscope (JEOL Ltd., Tokyo, Japan) operated at 200 kV. The mass spectra were acquired using the Autoflex laser desorption/ionization-time-of-flight mass spectrometry (LDI-TOF MS) (Bruker Daltonics, Germany). The Fourier transform infrared (FT-IR) spectra were measured using a PerkinElmer spectrum 100 FT-IR spectrometer (PerkinElmer Inc., USA) with KBr pellets. The lab-made dark-field microscope system consisted of an Olympus IX71 inverted microscope (Tokyo, Japan), a 100 W halogen lamp, a condenser (IX-ULWCD, Olympus, Tokyo, Japan), an objective (40 $\times$ ; numerical apertures = 0.75), and a digital camera (DP70, Olympus, Tokyo, Japan). Thermogravimetric analysis (TGA) were performed on a TGA 4000 analyzer (PerkinElmer Inc., USA).

Fluorescence lifetime was carried out using a time-correlated single photon counting system (Time-Harp 200, PicoQuant GmbH, Berlin, Germany) equipped with a pulsed diode laser at 390 nm (tens of ps pulse-width). The fluorescence decay curve was fitted by an exponential function:

$$I(t) = \sum_{i=1}^n A_i e^{-t/\tau_i}$$

where  $A_i$  represents the amplitude corresponding to the lifetime  $\tau_i$  in the intensity decay;  $I(t)$  represents the fluorescence intensity decay. The fluorescence decay curve of PDs was best fitted to a double exponential function.

## 2.4 Fluorescent detection of $\text{Fe}^{3+}$ .

Stock solutions of  $\text{Fe}^{3+}$  and metal ions were prepared in 10 mM Tris-HCl buffer at  $\text{pH} 4.0$ .  $\text{Fe}^{3+}$  (990  $\mu\text{L}$ , 1–50  $\mu\text{M}$ ) and metal

ions (990  $\mu\text{L}$ , 50  $\mu\text{M}$ ) were separately incubated with a solution of PDs (10  $\mu\text{L}$ ) at ambient temperature within 5 min. The fluorescence spectra of the resulting solutions were recorded at an excitation wavelength of 330 nm.

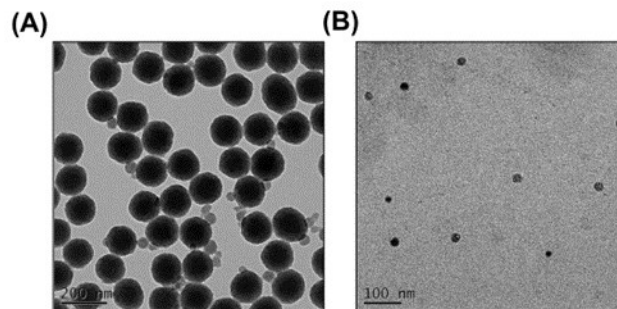


**Fig. 1.** (A) TEM images of (A) polydopamine nanoparticles and (B) PDs.

## 3. Results and discussion

### 3.1 Reactivity of Hydroxyl Radicals toward Polydopamine Nanoparticles.

Polydopamine nanoparticles were prepared through neutralization of dopamine hydrochloride with  $\text{NaOH}$  similar to previous reports.<sup>25</sup> Under this condition, the extensive 5,6-dihydroxyindole breakdown did not occur during polydopamine synthesis and nanoparticle formation. The mechanism for the formation of polydopamine nanoparticles relies on the spontaneous oxidation of dopamine in air. Ariga and colleagues used electron spin resonance to demonstrate the dissociation of  $\text{H}_2\text{O}_2$  into hydroxyl radicals at a high  $\text{NaOH}$  concentration.<sup>26, 27</sup> Therefore, in the presence of a mixture of  $\text{H}_2\text{O}_2$  and  $\text{NaOH}$  ( $\text{pH} \sim 10$ ), the as-prepared polydopamine nanoparticles reacted with hydroxyl radicals at  $100^\circ\text{C}$  for 30 min. To demonstrate the hydroxyl-radical-mediated degradation of polydopamine nanoparticles to PDs, the products obtained from the reaction of polydopamine nanoparticles with hydroxyl radicals were examined using TEM, DFM, and TGA. **Fig. 1** depicts TEM images of polydopamine nanoparticles and PDs with average diameters of  $139 \pm 10$  and  $22 \pm 3$  nm, respectively. DFM was used to observe the Rayleigh scattering of polydopamine nanoparticles and PDs. We note that DFM was sensitive in detecting the Rayleigh light scattering of particles.<sup>28</sup> The DFM images of the polydopamine nanoparticles contain intense orange-colored spots because the particles exhibited strong Rayleigh scattering (**Fig. S1**, ESI). By contrast, the PDs were too small for Rayleigh scattering to be observed. TGA was performed to evaluate the thermal stability of polydopamine nanoparticles and PDs. When the temperature was varied from room temperature to  $500^\circ\text{C}$ , the weight loss rate of polydopamine nanoparticles was slower than that of PDs (**Fig. S2**, ESI). Because the thermal stability of a polymeric material largely relies on the degree of crosslinking of the polymer,<sup>29</sup> we suggest that polydopamine nanoparticles contain more repeated units of 5,6-dihydroxyindole than PDs.<sup>30</sup> These results clearly indicated that hydroxyl radicals can induce the degradation of polydopamine to PDs. Previous studies have reported similar results showing that hydroxyl radicals were efficient in decomposing polymeric materials,<sup>31</sup> reduced graphene oxide,<sup>32</sup> and DNA.<sup>33</sup> FT-IR spectroscopy and LDI-TOF MS were used to

determine the possible chemical structures of PDs. The FT-IR spectrum of polydopamine nanoparticles exhibited two major bands at 1615 and 3420  $\text{cm}^{-1}$  (Fig. S3A, ESI), which originated from the stretching vibrations of C=C and O–H, respectively. This result is consistent with previous FTIR measurements of polydopamine.<sup>15, 25, 34, 35</sup> In addition, two major bands corresponding to the stretching vibrations of C=C and O–H were observed in the spectrum of PDs (Fig. S3B, ESI), suggesting that the functional groups of polydopamine nanoparticles resemble those of PDs. An additional peak centered at 1397  $\text{cm}^{-1}$  was attributed to the O–H deformation vibration.

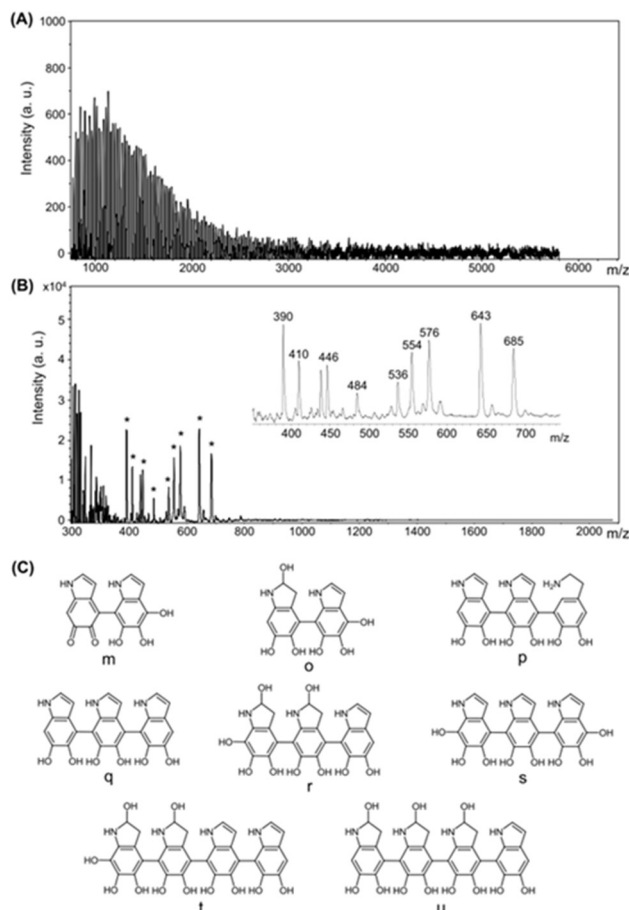


**Fig. 2.** LDI-TOF mass spectra of (A) polydopamine nanoparticles and (B) PDs. (C) Possible chemical structures of the fragments of PDs.

Compared to polydopamine nanoparticles, the FT-IR spectrum of PDs shows a less pronounced peak. This could be attributed to the fact that polydopamine nanoparticles have a higher degree of oligomerization and self-assembly than PDs. A similar phenomenon was observed in the study of the coating of polydopamine on citrate-capped gold nanoparticles.<sup>15</sup> Because the detection of analyte by LDI-MS can induce its fragmentation, we suggest that the analysis of PDs by LDI-MS could provide the information about their possible chemical composition.<sup>36</sup> Compared to matrix-assisted laser desorption/ionization mass spectrometry, the detection of analyte by LDI-MS avoids the interference from organic matrix.<sup>37</sup> The mass spectrum of polydopamine nanoparticles consisted of a broad range of peaks

between  $m/z$  800 and 3000 with a spacing of  $m/z$  24 (Fig. 2A). Dreyer and colleagues reported a similar analysis result; polydopamine-coated steel produced a series of peaks between  $m/z$  888 and 3500 with a spacing of  $m/z$  24.<sup>34</sup> However, this spacing is inconsistent with the proposed repeat units of 5,6-dihydroxyindole in polydopamine nanoparticles. This phenomenon is not clearly understood. By contrast, the mass spectrum of PDs consisted of several peaks at  $m/z$  390, 410, 446, 484, 536, 554, 576, 643, and 685 corresponding to  $[m + 2K + OH]^+$ ,  $[o + 2K + OH]^+$ ,  $[p-H]^+$ ,  $[q + K]^+$ ,  $[r + K + 3OH]^+$ ,  $[s + 2K + 2OH]^+$ ,  $[r + 2K + 3OH]^+$ ,  $[t + H + 3OH]^+$ , and  $[u + K + 3OH]^+$ , respectively, which possibly originated from the PD fragments (Fig. 2B). Fig. 2C shows the possible chemical structures of  $m$ ,  $o$ ,  $p$ ,  $q$ ,  $r$ ,  $s$ ,  $t$ , and  $u$ , suggesting that the  $\text{H}_2\text{O}_2$ -induced decomposition of polydopamine nanoparticles could be attributed to the addition of hydroxyl groups to the activated double bonds of their pyrrole ring and aromatic ring. Because mass spectrometric data do not provide unambiguous evidence for the exact chemical structure, the addition of hydroxyl groups at the exact positions of dopamine and 5,6-dihydroxyindole remain unknown. According to the aforementioned results, we concluded that three processes occurred during the synthesis of PDs (Fig. 3): (1) Dopamine was oxidized to 5,6-dihydroxyindole under alkaline conditions (20 mM NaOH) with oxygen as the oxidant; (2) the polymerization of dopamine and 5,6-dihydroxyindole immediately occurred through intra- and intermolecular cross-linking reactions, resulting in the formation of polydopamine nanoparticles; and (3) the reaction between NaOH and  $\text{H}_2\text{O}_2$  produced hydroxyl radicals, which were efficient to decompose polydopamine nanoparticles to PDs via the addition of hydroxyl groups to 5,6-dihydroxyindole units of polydopamine units.

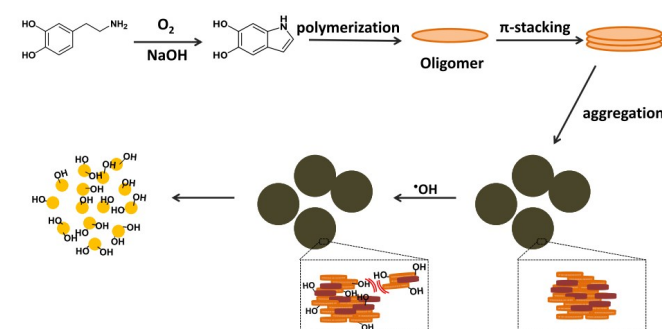


**Fig. 3.** Schematic illustration of the synthesis procedure for PDs

### 3.2 Optical properties and stability of PDs.

Compared with the absorption spectrum of dopamine (Curve a in Fig. 4A), the spectrum of polydopamine nanoparticles showed broad adsorption from 200 to 500 nm because of the formation of 5,6-dihydroxyindole units (Curve b in Fig. 4A).<sup>38-40</sup> In addition, polydopamine nanoparticles showed relatively less intense absorption at 280 nm, suggesting the presence of a substantial proportion of dopamine in polydopamine nanoparticles. The same feature was observed in previous studies.<sup>38, 41</sup> Following the addition of  $\text{H}_2\text{O}_2$  to a solution of polydopamine nanoparticles in the presence of NaOH, the formed PDs exhibited relatively less intense absorption from 200 to 500 nm, and the peak at 280 nm disappeared (Curve c in Fig. 4A), indicating that PDs contain a lower proportion of 5,6-dihydroxyindole and dopamine units. Interestingly, the

absorption spectrum of PDs is highly similar to that of eumelanin.<sup>42</sup> In addition, the maximum fluorescence of eumelanin can be varied by changing the excitation wavelength.<sup>42-44</sup> Motivated by these results, we investigated the fluorescent properties of PDs. Upon excitation at 330 nm, the emission band of dopamine was centered at approximately 375 nm (Curve a in Fig. 4B). At the same excitation wavelength, the maximal emission of polydopamine nanoparticles and PDs shifted to 440 nm (Curves b and c in Fig. 4B). This difference was attributed to the oxidation of dopamine to 5,6-dihydroxyindole. In contrast to polydopamine nanoparticles, PDs exhibited extremely strong fluorescence. Previous studies have reported the presence of an extended  $\pi$ - $\pi$  stacking interaction between the oligomeric units in a polydopamine film<sup>34, 45</sup> and polydopamine nanoparticles.<sup>39</sup> Thus, the particle size of PDs was considerably smaller than that of polydopamine nanoparticles, suggesting that PDs had a lower degree of  $\pi$ - $\pi$  stacking interaction. Moreover, the presence of additional hydroxyl groups in PDs can effectively prevent the conjugated backbone from  $\pi$ - $\pi$  stacking. Because  $\pi$ - $\pi$  stacking interaction can induce fluorescence quenching,<sup>46-48</sup> strong fluorescence by the PDs was observed.

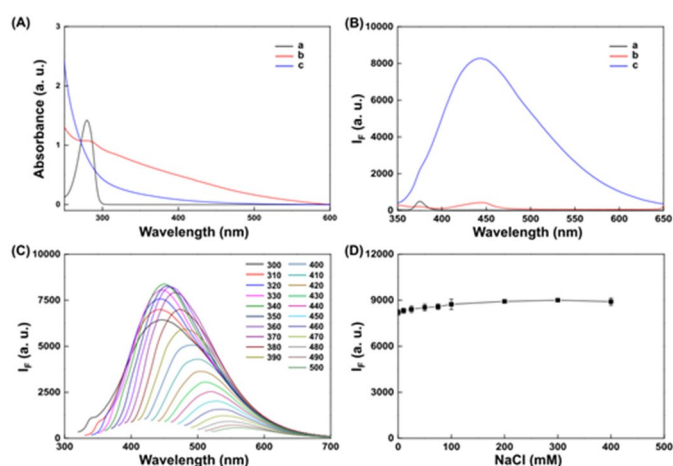


**Fig. 4.** (A) Absorption and (B) fluorescence spectra of (a) dopamine, (b) polydopamine nanoparticles, and (c) PDs. (C) Fluorescence spectra of PDs with excitation of different wavelength. (D) Effect of the NaCl concentration on the fluorescence intensity at 440 nm of PDs. (B, D) The excitation wavelength was set at 330 nm.

When the excitation wavelength was increased from 300 to 500 nm, the maximal emission shifted from 447 to 556 nm (Fig. 4C). This result indicated that the maximal emission of PDs strongly depends on the excitation wavelength. Because PDs contain dopamine, 5,6-dihydroxyindole, and trihydroxyindole units, oligomerization and self-assembly of these units formed a series of unique species. Each species had different highest occupied molecular orbital–lowest unoccupied molecular orbital energy gaps in the UV to visible range, leading to broad adsorption and variation in color emission according to the excitation wavelength. Similarly, eumelanin, which contains 5,6-dihydroxyindole and 5,6-dihydroxyindole-2-carboxylic acid units, exhibited an excitation-dependent emission wavelength behavior.<sup>42</sup> To confirm the formation of a series of chemically distinct species, lifetime values of blue- and green-emitting PDs

were obtained by numerically fitting the fluorescence at 480 nm (excitation at 390 nm) and 542 nm (excitation at 485 nm), respectively. Blue-emitting PDs exhibited two lifetimes of 3.8 ns (77%) and 10.8 ns (23%) (Fig. S4, ESI), and green-emitting PDs exhibited two lifetimes of 4.0 ns (69%) and 9.4 ns (31%) (Fig. S5, ESI). The short fluorescence lifetime was approximately the same for the two excitation wavelengths. The difference in the long fluorescence lifetime suggested that green-emitting PDs had a higher degree of oligomerization and self-assembly than blue-emitting PDs. This was attributed to the decrease in the energy gaps in such PDs as the degree of oligomerization and self-assembly of dopamine, 5,6-dihydroxyindole, and trihydroxyindole units increased. In addition, the observed lifetime of PDs in nanoseconds implied that the synthesized PDs are suited for optoelectronic and biological applications. The most intense fluorescence emission occurred at 440 nm when a solution of PDs was excited at 330 nm. At the same excitation wavelength, the quantum yield of PDs was determined to be 1.2% by using quinine sulfate as the reference (Fig. S6, ESI).

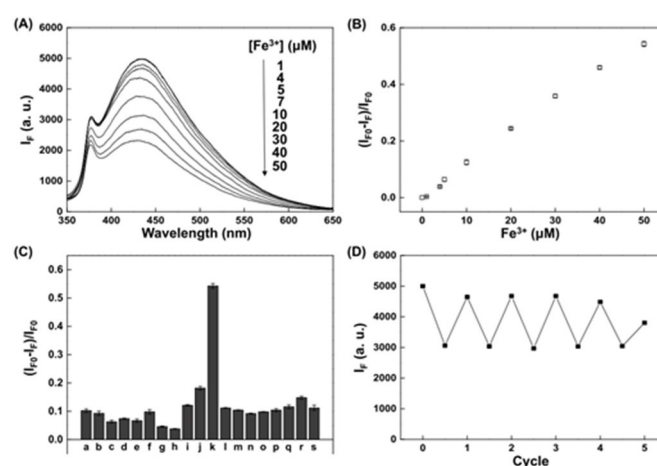


**Fig. 5.** (A) Change in fluorescence spectra of PDs in the presence of increasing concentrations of  $\text{Fe}^{3+}$ . (B) A plot of the  $(I_{F0} - I)/I_{F0}$  value at 440 nm versus the  $\text{Fe}^{3+}$  concentration. (C) The  $(I_{F0} - I)/I_{F0}$  value at 440 nm obtained from the addition of (a)  $\text{Li}^+$ , (b)  $\text{Na}^+$ , (c)  $\text{K}^+$ , (d)  $\text{Be}^{2+}$ , (e)  $\text{Mg}^{2+}$ , (f)  $\text{Ca}^{2+}$ , (g)  $\text{Sr}^{2+}$ , (h)  $\text{Mn}^{2+}$ , (i)  $\text{Ba}^{2+}$ , (j)  $\text{Fe}^{2+}$ , (k)  $\text{Fe}^{3+}$ , (l)  $\text{Co}^{2+}$ , (m)  $\text{Ni}^{2+}$ , (n)  $\text{Cu}^{2+}$ , (o)  $\text{Zn}^{2+}$ , (p)  $\text{Cd}^{2+}$ , (q)  $\text{Hg}^{2+}$ , (r)  $\text{Pb}^{2+}$ , and (s)  $\text{Cr}^{3+}$  to a solution of PDs. The concentrations of  $\text{Fe}^{3+}$  and other metal ions are 10 and 50  $\mu\text{M}$ , respectively. (D) Reversible switching of PDs between the ON and OFF states through the alternating addition of 10  $\mu\text{M}$   $\text{Fe}^{3+}$  and 30  $\mu\text{M}$  pyrophosphate. (A–D) A mixture of PDs and metal ion was incubated in 10 mM Tris-HCl buffer at pH 7.0 for 5 min. The error bar represent standard deviations based on three independent measurements.

The stability of PDs was tested by varying the NaCl concentration (Fig. 4D). When the NaCl concentration was varied from 0 to 400 mM in a solution of 10 mM phosphate (pH 7.0), a rare change in the fluorescence intensity of PDs at 440 nm suggested that the PDs were extremely stable under high-ionic-strength conditions. Fig. S7 (ESI) shows that the fluorescence of PDs was insensitive to pH change from pH 3 to 12, indicating that the PDs were stable in a wide pH range. These results suggested that PDs can sense molecules of interest under physiological conditions. To confirm hydroxyl radical-induced

production of fluorescent PDs, the Fenton reaction of polydopamine nanoparticles proceeded in an aqueous solution containing 1 M H<sub>2</sub>O<sub>2</sub> and 10 mM Fe(II) at ambient temperature for 2 h. Note that the Fenton reaction produces hydroxyl radicals via Fe(II)-mediated reduction of H<sub>2</sub>O<sub>2</sub>.<sup>4</sup> The absorption and fluorescence spectra of the obtained products resembled those of PDs (Fig. S8 and S9, ESI), suggesting that hydroxyl radicals indeed break down polydopamine nanoparticles into fluorescent PDs.

### 3.3 Application of PDs as optical sensors.

The high levels of Fe<sup>3+</sup> in drinking water cause severe public health risks because Fe<sup>3+</sup> behaves as a surrogate for other heavy metal ions. In addition, exposure to high levels of Fe<sup>3+</sup> causes severe vomiting, abdominal pain, diarrhea, and heart and liver damage,<sup>23</sup> whereas Fe<sup>3+</sup> deficiency induces anemia.<sup>49</sup> Thus, the development of an optical sensor for sensing Fe<sup>3+</sup> is of considerable interest. Previous studies reported that Fe<sup>3+</sup> is efficient in linking catechol-containing polymers through the formation of catechol-Fe<sup>3+</sup> complexes.<sup>50, 51</sup> We inferred that the catechol groups on the PD surface can coordinate with Fe<sup>3+</sup>, resulting in the fluorescence quenching of PDs with Fe<sup>3+</sup> acting as an electron acceptor. Because Fe<sup>3+</sup> precipitates at an alkaline pH ( $K_{sp}$  of Fe(OH)<sub>3</sub> =  $6 \times 10^{-38}$ ), PDs were incubated with Fe<sup>3+</sup> at a low pH (10 mM Tris-HCl, pH 4.0). As the Fe<sup>3+</sup> concentration was increased, the fluorescence spectrum of PDs showed a gradual decrease in fluorescence at 440 nm (Fig. 5A). A plot of the  $(I_{F0} - I_F)/I_{F0}$  value versus the Fe<sup>3+</sup> concentration is shown in the inset of Fig. 5B, and a linear relationship was observed from 1 to 50 μM ( $R^2 = 0.9958$ ). Here,  $I_{F0}$  and  $I_F$  are the fluorescence intensity of PDs at 440 nm in the absence and presence of Fe<sup>3+</sup>, respectively. The limit of detection at a signal-to-noise ratio of 3 for Fe<sup>3+</sup> was calculated to be 0.3 μM, which is lower than the secondary maximal contaminant level (0.3 mg/L, 5.4 μM) of iron permissible in drinking water, as specified by the United States Environmental Protection Agency. Furthermore, the selectivity of PDs toward Fe<sup>3+</sup> was tested, and Fig. 5C shows that changes in the  $(I_{F0} - I_F)/I_{F0}$  value of PDs occurred within 10 min after Fe<sup>3+</sup> and other metal ions were added separately. Only Fe<sup>3+</sup> caused a marked increase in  $(I_{F0} - I_F)/I_{F0}$ , showing that PDs are highly selective to Fe<sup>3+</sup>. This is primarily because the catechol groups of PDs can selectively coordinate with Fe<sup>3+</sup>.<sup>52-54</sup> Similarly, catechol-modified carbon dots were used for the fluorescent sensing of Fe<sup>3+</sup> through the formation of Fe<sup>3+</sup>-catechol complexes.<sup>55</sup> Pyrophosphate can complex with Fe<sup>3+</sup> to form Fe<sub>4</sub>(P<sub>2</sub>O<sub>7</sub>)<sub>3</sub>, suggesting that this probe can be reused for detecting Fe<sup>3+</sup>. Fig. 5D indicates that the alternative addition of Fe<sup>3+</sup> and pyrophosphate enabled the fluorescence intensity of PDs at 440 nm to alternate between on and off states. This repeated switching behavior suggested that PDs exhibit satisfactory reusability for detecting Fe<sup>3+</sup>. Although PDs do not provide the greatest sensitivity toward Fe<sup>3+</sup> among other Fe<sup>3+</sup> sensors (Table S1, ESI), the synthesis of PDs is relatively simple, low cost, green, and easily upscalable. We then clarified the mechanism of the Fe<sup>3+</sup>-induced fluorescence quenching of PDs. Because the emission spectrum of PDs (i.e., donor) showed minimal spectral overlap with the absorption spectrum of Fe<sup>3+</sup> (i.e., acceptor), we precluded the fluorescence resonance energy transfer<sup>56</sup> and the Dexter energy transfer.<sup>57</sup> The reduction potential of Fe<sup>3+</sup> to Fe<sup>2+</sup> is +0.57 V (vs Ag/AgCl), indicating that Fe<sup>3+</sup> has a strong ability to capture an electron. A previous study reported that the oxidation potentials of 5,6-dihydroxyindole and dopamine in polydopamine were -0.04 and +0.2 V (vs Ag/AgCl), respectively.<sup>58</sup> Apparently, the reduction potential of Fe<sup>3+</sup> is

sufficient to cause electron transfer from the excited state of PDs (i.e., donor) to the unfilled d shell of Fe<sup>3+</sup> (i.e., acceptor). Many studies have reported that Fe<sup>3+</sup> can cause electron-transfer-induced fluorescence quenching of a fluorescent probe through the formation of a complex between Fe<sup>3+</sup> and the fluorescent probe.<sup>59</sup> According to previous studies and our present findings, we propose that the mechanism of Fe<sup>3+</sup>-induced fluorescence quenching of PDs involves oxidative photoinduced electron transfer from the excited state of PDs to an unfilled d shell of Fe<sup>3+</sup>.

### Conclusions

We, for the first time, demonstrated the facile synthesis of blue-emitting PDs (quantum yield: approximately 1.2%) through hydroxyl-radical-induced degradation of polydopamine nanoparticles. The PDs may have contained dopamine, 5,6-dihydroxyindole, and trihydroxyindole units, resulting in a broad adsorption and excitation-wavelength-dependent emission behavior. Because Fe<sup>3+</sup> can complex with the catechol groups of PDs, PDs were used in the fluorescence turn-off detection of Fe<sup>3+</sup> through oxidative photoinduced electron transfer. PDs can mimic the set–reset logic function through the alternative addition of Fe<sup>3+</sup> and pyrophosphate.

### Acknowledgements

We would like to thank the Ministry of Science and Technology (NSC 100-2628-M-110-001- MY4) for the financial support of this study.

### Notes and references

<sup>a</sup>Department of Chemistry, National Sun Yat-sen University, Kaohsiung, Taiwan. Fax: 011-886-7-3684046; E-mail: tsengwl@mail.nsysu.edu.tw  
<sup>b</sup>School of Pharmacy, College of Pharmacy, Kaohsiung Medical University, Taiwan. Fax: 011-886-7-3684046; E-mail: tsengwl@mail.nsysu.edu.tw

† Electronic Supplementary Information (ESI) available: Experimental procedures on prepared compounds and Fig. S1-S12]. See DOI: 10.1039/b000000x/

- N. Boens, V. Leen and W. Dehaen, *Chem. Soc. Rev.*, 2012, **41**, 1130-1172.
- K. P. Carter, A. M. Young and A. E. Palmer, *Chem. Rev.*, 2014, **114**, 4564-4601.
- N. Basaric, M. Baruah, W. W. Qin, B. Metten, M. Smet, W. Dehaen and N. Boens, *Org. Biomol. Chem.*, 2005, **3**, 2755-2761.
- X. Michalet, F. F. Pinaud, L. A. Bentolila, J. M. Tsay, S. Doose, J. J. Li, G. Sundaresan, A. M. Wu, S. S. Gambhir and S. Weiss, *Science*, 2005, **307**, 538-544.
- P. J. G. Luo, F. Yang, S. T. Yang, S. K. Sonkar, L. J. Yang, J. J. Broglie, Y. Liu and Y. P. Sun, *Rsc Adv.*, 2014, **4**, 10791-10807.
- X. Y. Cheng, S. B. Lowe, P. J. Reece and J. J. Gooding, *Chem. Soc. Rev.*, 2014, **43**, 2680-2700.
- M. Melinn and H. McLaughlin, *Immunology*, 1986, **58**, 197-202.
- G. Rousserie, A. Sukhanova, K. Even-Desrumeaux, F. Fleury, P. Chames, D. Baty, V. Oleinikov, M. Pluot, J. H. M. Cohen and I. Nabiev, *Crit. Rev. Oncol. Hemat.*, 2010, **74**, 1-15.
- H. Li, Z. Kang, Y. Liu and S.-T. Lee, *J. Mater. Chem.*, 2012, **22**, 24230-24253.
- W. Shi, X. Li and H. Ma, *Angew. Chem. Int. Ed.*, 2012, **51**, 6432-6435.
- J. Shen, Y. Zhu, X. Yang and C. Li, *Chem. Commun.*, 2012, **48**, 3686-3699.
- L. Polavarapu, M. Manna and Q. H. Xu, *Nanoscale*, 2011, **3**, 429-434.
- C. Wu, S. J. Hansen, Q. Hou, J. Yu, M. Zeigler, Y. Jin, D. R. Burnham, J. D. McNeill, J. M. Olson and D. T. Chiu, *Angew. Chem. Int. Ed.*, 2011, **50**, 3430-3434.
- C. Wu, T. Schneider, M. Zeigler, J. Yu, P. G. Schiro, D. R. Burnham, J. D.

- McNeill and D. T. Chiu, *J. Am. Chem. Soc.*, 2010, **132**, 15410-15417.
15. X. Liu, J. Cao, H. Li, J. Li, Q. Jin, K. Ren and J. Ji, *ACS Nano*, 2013, **7**, 9384-9395.
16. M. Zhang, X. Zhang, X. He, L. Chen and Y. Zhang, *Nanoscale*, 2012, **4**, 3141-3147.
17. S. M. Kang, I. You, W. K. Cho, H. K. Shon, T. G. Lee, I. S. Choi, J. M. Karp and H. Lee, *Angew. Chem. Int. Ed.*, 2010, **49**, 9401-9404.
18. M. Nurunnabi, Z. Khatun, M. Nafiujjaman, D. G. Lee and Y. K. Lee, *ACS Appl. Mater. Interfaces*, 2013, **5**, 8246-8253.
19. H. Lee, S. M. Dellatore, W. M. Miller and P. B. Messersmith, *Science*, 2007, **318**, 426-430.
20. F. Bernsmann, V. Ball, F. Addiego, A. Ponche, M. Michel, J. J. Gracio, V. Toniazzo and D. Ruch, *Langmuir*, 2011, **27**, 2819-2825.
21. X. Zhang, S. Wang, L. Xu, L. Feng, Y. Ji, L. Tao, S. Li and Y. Wei, *Nanoscale*, 2012, **4**, 5581-5584.
22. X. Chen, Y. Yan, M. Mullner, M. P. van Koevorden, K. F. Noi, W. Zhu and F. Caruso, *Langmuir*, 2014, **30**, 2921-2925.
23. F. O. Omara and B. R. Blakley, *J. Nutr.*, 1993, **123**, 1649-1655.
24. X. F. Wang, Y. Zhou, J. J. Xu and H. Y. Chen, *Adv. Funct. Mater.*, 2009, **19**, 1444-1450.
25. K. Y. Ju, Y. Lee, S. Lee, S. B. Park and J. K. Lee, *Biomacromolecules*, 2011, **12**, 625-632.
26. Y. Yoshimura, T. Inomata, H. Nakazawa, H. Kubo, F. Yamaguchi and T. Ariga, *J. Agric. Food Chem.*, 1999, **47**, 4653-4656.
27. F. Yamaguchi, Y. Yoshimura, H. Nakazawa and T. Ariga, *J. Agric. Food Chem.*, 1999, **47**, 2544-2548.
28. R. Jin, Y. Cao, C. A. Mirkin, K. L. Kelly, G. C. Schatz and J. G. Zheng, *Science*, 2001, **294**, 1901-1903.
29. A. Bigi, G. Cojazzi, S. Panzavolta, K. Rubini and N. Roveri, *Biomaterials*, 2001, **22**, 763-768.
30. S. Xiong, Y. Wang, J. Yu, L. Chen, J. Zhu and Z. Hu, *J. Mater. Chem. A*, 2014, **2**, 7578-7587.
31. S. A. Ali, S. P. Zhong, P. J. Doherty and D. F. Williams, *Biomaterials*, 1993, **14**, 648-656.
32. J. G. Radich and P. V. Kamat, *ACS Nano*, 2013, **7**, 5546-5557.
33. M. S. Cooke, M. D. Evans, M. Dizdaroglu and J. Lunec, *FASEB J.*, 2003, **17**, 1195-1214.
34. D. R. Dreyer, D. J. Miller, B. D. Freeman, D. R. Paul and C. W. Bielawski, *Langmuir*, 2012, **28**, 6428-6435.
35. K. Ai, Y. Liu, C. Ruan, L. Lu and G. M. Lu, *Adv. Mater.*, 2013, **25**, 998-1003.
36. S. Acevedo, J. M. Cordero, H. Carrier, B. Bouyssiere and R. Lobinski, *Energ. Fuel.*, 2009, **23**, 842-848.
37. Y. E. Silina and D. A. Volmer, *The Analyst*, 2013, **138**, 7053-7065.
38. N. F. Della Vecchia, R. Avolio, M. Alfè, M. E. Errico, A. Napolitano and M. d'Ischia, *Adv. Funct. Mater.*, 2013, **23**, 1331-1340.
39. X. Yu, H. Fan, Y. Liu, Z. Shi and Z. Jin, *Langmuir*, 2014, **30**, 5497-5505.
40. M. L. Tran, B. J. Powell and P. Meredith, *Biophys. J.*, 2006, **90**, 743-752.
41. J. Liebscher, R. Mrowczynski, H. A. Scheidt, C. Filip, N. D. Hadade, R. Turcu, A. Bende and S. Beck, *Langmuir*, 2013, **29**, 10539-10548.
42. A. Huijser, A. Pezzella and V. Sundstrom, *Phys. Chem. Chem. Phys.*, 2011, **13**, 9119-9127.
43. J. M. Gallas and M. Eisner, *Photochem. Photobiol.*, 1987, **45**, 595-600.
44. S. Kozikowski, L. Wolfram and R. Alfano, *IEEE J. Quantum Electron.*, 1984, **20**, 1379-1382.
45. S. Hong, Y. S. Na, S. Choi, I. T. Song, W. Y. Kim and H. Lee, *Adv. Funct. Mater.*, 2012, **22**, 4711-4717.
46. C. Pan, K. Sugiyasu, Y. Wakayama, A. Sato and M. Takeuchi, *Angew. Chem. Int. Ed.*, 2013, **52**, 10775-10779.
47. S. Bevers, S. Schutte and L. W. McLaughlin, *J. Am. Chem. Soc.*, 2000, **122**, 5905-5915.
48. Z. Xu, N. J. Singh, J. Lim, J. Pan, H. N. Kim, S. Park, K. S. Kim and J. Yoon, *J. Am. Chem. Soc.*, 2009, **131**, 15528-15533.
49. L. H. Allen, *J. Nutr.*, 2002, **132**, 813S-819S.
50. N. Holten-Andersen, M. J. Harrington, H. Birkedal, B. P. Lee, P. B. Messersmith, K. Y. Lee and J. H. Waite, *Proc. Natl. Acad. Sci. U. S. A.*, 2011, **108**, 2651-2655.
51. M. Krogsgaard, M. A. Behrens, J. S. Pedersen and H. Birkedal, *Biomacromolecules*, 2013, **14**, 297-301.
52. C. Queirós, A. M. G. Silva, S. C. Lopes, G. Ivanova, P. Gameiro and M. Rangel, *Dyes Pigments*, 2012, **93**, 1447-1455.
53. Z. D. Liu and R. C. Hider, *Coord. Chem. Rev.*, 2002, **232**, 151-171.
54. R. K. Jackson, Y. Shi, X. Yao and S. C. Burdette, *Dalton Trans.*, 2010, **39**, 4155-4161.
55. K. Qu, J. Wang, J. Ren and X. Qu, *Chemistry*, 2013, **19**, 7243-7249.
56. A. Zeug, A. Woehler, E. Neher and E. G. Ponimaskin, *Biophys. J.*, 2012, **103**, 1821-1827.
57. D. L. Dexter, *J. Chem. Phys.*, 1953, **21**, 836-850.
58. R. A. Zangmeister, T. A. Morris and M. J. Tarlov, *Langmuir*, 2013, **29**, 8619-8628.
59. S. K. Sahoo, D. Sharma, R. K. Bera, G. Crisponi and J. F. Callan, *Chem. Soc. Rev.*, 2012, **41**, 7195-7227.